Off-centre dynamic Jahn-Teller effect studied by electron spin relaxation of Cu^{2+} ions in SrF_2 crystal

2000 J. Phys.: Condens. Matter 12 1855

(http://iopscience.iop.org/0953-8984/12/8/328)

J. Phys.: Condens. Matter **12** (2000) 1855–1866. Printed in the UK PII: S0953-8984(00)05574-0

Off-centre dynamic Jahn–Teller effect studied by electron spin relaxation of Cu^{2+} ions in SrF_2 crystal

S K Hoffmann†§ and V A Ulanov‡

† Institute of Molecular Physics, Polish Academy of Sciences, Smoluchowskiego 17, PL-60-179 Poznan, Poland

‡ Physical Technical Institute, Russian Academy of Sciences, Sibirski Trakt 10/7, 420029 Kazan, Russia

E-mail: skh@ifmpan.poznan.pl

Received 28 June 1999, in final form 11 November 1999

Abstract. Temperature cw-EPR and pulsed EPR electron spin echo experiments were performed for a low concentration of Cu^{2+} ions in cubic SrF_2 crystals. The well resolved EPR spectrum at low temperatures (below 30 K) with parameters $g_\parallel = 2.493$, $g_\perp = 2.083$, $A_\parallel = 121$, $A_\perp = 8.7$, $A_\parallel(^{19}\mathrm{F}) = 135$, $A_\parallel(^{19}\mathrm{F}) = 33.0$ (A-values in 10^{-4} cm^{-1}) is transformed continuously into a single broad line above 225 K on heating, due to the g-factor shift and EPR line broadening. These data along with the angular variation EPR data are described in terms of a pseudo-Jahn–Teller effect of $(T_{2g} + A_{2u}) \otimes (a_{1g} + e_g + t_{1u})$ type producing six off-centre positions of the Cu^{2+} ion in the fluorine cube. Above 30 K a two-step averaging g-factor process occurs and is governed by vibronic dynamics between potential wells of the off-centre positions. This dynamics governs the electron spin relaxation in the whole temperature range. The electron spin–lattice relaxation rate $1/T_1$ grows rapidly by six orders of magnitude in the temperature range 30–100 K and is determined by the Orbach-type process with excitations to two excited vibronic levels of energy 83 and 174 cm^{-1}. For higher temperatures the relaxation is dominated by overbarrier jumps leading to the isotropic EPR spectrum above 225 K. The phase memory time T_M has the rigid lattice value 3.5 μs determined by nuclear spectral diffusion and its temperature variation is governed by the vibronic dynamics indicating that the excitations between vibronic levels produce a dephasing of the electron spin precessional motion.

1. Introduction

Various paramagnetic centres introduced, for EPR studies, into cubic fluorite type crystal structures (CaF_2, CdF_2, SrF_2, BaF_2, $SrCl_2$) substitute divalent host metals (such as Cu^{2+}, Ag^{2+}, Ni^{+}, Cr^{2+}, Cr^{3+} [1–8]; Sc^{2+}, La^{2+} [9]; atomic hydrogen H^0 [10, 11]) or occupy anionic sites (like O^- or OH^-) [12, 13]. The transition metal ion behaviour in fluorite structures prior to 1980 has been reviewed in [14]. The common feature of the first type of centre is that under some conditions the Jahn–Teller effect accompanied by lattice polarization effects can produce a displacement of the guest cation to an off-centre position along the fourfold symmetry axes of the fluoride or chloride cube. The displacement from the centre of the cube is relatively large and reaches 0.135 nm for Cu^{2+} in $SrCl_2$ [4]. EPR studies show that Cu^{2+} centres are static in chloride crystals over a broad temperature range, whereas the EPR parameters are strongly temperature dependent in fluorite lattices. The latter behaviour was explained as a result of temperature induced movement in a multiwell potential of the off-centre positions.

§ Addressee for correspondence: Professor S K Hoffmann.

0953-8984/00/081855+12$30.00

The Jahn–Teller effect producing a displacement of a paramagnetic ion from the geometric centre of the coordination sphere towards off-centre positions is a special case of the vibronic effects in stereochemistry [15]. In most cases the vibronic coupling produces a deformation of the coordination polyhedron by ligand atom displacements. Under special conditions, however, a displacement of the central metal ion can be preferred. It can appears when the impurity ion is far lighter than the ligand atoms [16], when metal–ligand coordination bonding is weaker than ligand–lattice bondings, or when there exists a vibronic mixing of the excited electronic states to the high-symmetry ground state by low-symmetry nuclear motions stabilizing the central ion displacements by formation of a new covalency [15]. Such behaviour, which is pseudo-Jahn–Teller in origin, is responsible for ferroelectricity and displacive structural phase transitions in perovskite structures [17].

In addition to the off-centre type Jahn–Teller effect observed for Cu^{2+} in BaF_2 [3, 4] the *normal* dynamic Jahn–Teller effect was claimed to be responsible for an appearance of the quadrupole interaction of Sc^{2+} and La^{2+} ions detected as forbidden EPR lines in SrF_2 and $SrCl_2$ crystals [9] or to determine the dynamical effects observed for O^- impurity in CaF_2 crystals [12].

In this paper we show that variable temperature EPR data for Cu^{2+} in SrF_2 indicate that the Jahn–Teller effect produces six off-centre positions of copper(II) ions. But we pay attention mainly to the electron spin–lattice relaxation data collected by the electron spin echo technique. The problem of the influence of the Jahn–Teller dynamics on the electron spin–lattice relaxation is a poorly experimentally explored field although the theoretical predictions are well formulated [18, 19]. Experimental relaxation data were collected mainly for $E \otimes \varepsilon$ Jahn–Teller coupling of Cu^{2+} complexes in the doublet ground state of octahedral symmetry [20, 21 and references therein] although the spin–lattice relaxation in the triplet orbital T_{2g} state of $[Ti(H_2O)_6]^{3+}$ octahedra in methylammonium aluminum alum was studied below 4.2 K [22].

The problem if the Jahn–Teller effect can be the mechanism of the electron spin phase relaxation is even worse recognized. Temperature variations of the phase memory time T_M were measured by pulsed EPR for H^0 in SrF_2 [10] and theoretically described using a stochastic Liouville formalism describing a two-jump motion model [11]. In [12] it was shown that reorientations between Jahn–Teller distorted configurations of O^- in CaF_2 can be accompanied by a change in the phase of the unpaired electron precessional motion and such an effect was studied by the EPR saturation method at 4.2 K. The T_M and ESEEM spectroscopy data of Cu^{2+} and Mn^{2+} in $(NH_4)_2Mg(SO_4)_2.6H_2O$ crystals have shown an influence of the dynamical Jahn–Teller effect on phase relaxation and an existence of large vibronic clusters [20, 21, 23]. Moreover, the ESEEM spectroscopy of Cr^{2+} in SrF_2 [24] and CaF_2 [6] allowed us to propose a detailed model of the defect localization in the lattice.

In this paper we present the results of electron spin echo measurements of both the electron spin–lattice relaxation time T_1 and phase memory time T_M in a relatively broad temperature range, and show that temperature variations of the relaxation rates are due primarily to the dynamic Jahn–Teller effect within off-centre Cu^{2+} positions in the SrF_2 crystal.

2. Experimental details

Single crystals of SrF_2 were grown using the Bridgman technique in helium–fluorine gaseous atmosphere from SrF_2–metallic Cu melt in a graphite crucible. The crystals were elongated along the [110] direction with well developed (110) planes. The copper(II) ion content was determined from the intensity of the EPR spectrum as 1×10^{18} ions cm^{-3}.

Cw and pulsed EPR experiments were performed on a Bruker ESP 380E FT/CW spectrometer with dielectric TE_{001}-type resonator, equipped with a flowing helium Oxford

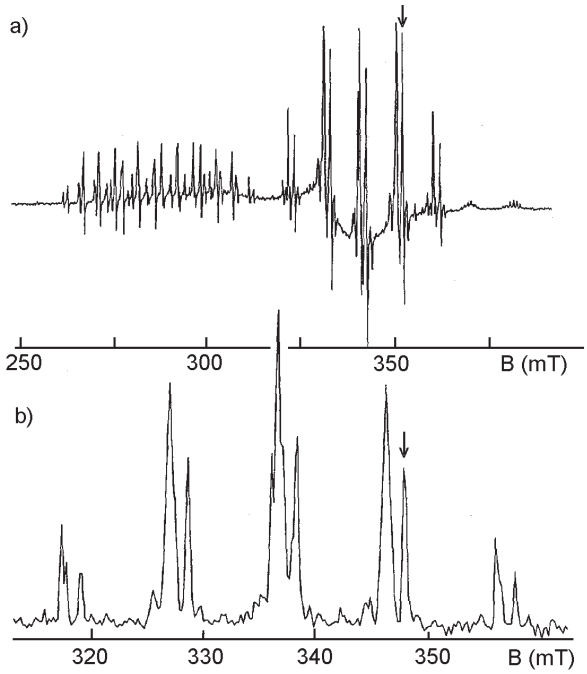

Figure 1. (a) Cw-EPR spectrum recorded along [001] direction at 11 K. The arrow shows the hfs line which was excited in pulsed EPR experiments. (b) Field swept electron spin echo spectrum of the perpendicular region of the cw-EPR spectrum. The broad background line is not observed due to its fast relaxation.

CF935 cryostat. Temperature variations of EPR spectra were recorded along the [001] direction where the spectrum was well resolved and simplified due to the crystal symmetry. At the same crystal orientation the pulsed EPR experiments were performed with excitation of the single EPR line in the perpendicular region of the spectrum as marked by the arrow in figure 1.

Electron spin relaxation times were measured using the electron spin echo (ESE) signal in the temperature range 10–84 K. For higher temperatures the ESE was nondetectable due to an increase in EPR line homogeneity. The Hahn type ESE was generated using 80 ns pulses with amplitude adjusted to obtain maximum echo amplitude and with initial interpulse distance 200 ns. The 80 ns pulse with 4.5 Gauss spectral width was able to excite the whole selected EPR line. Spin–lattice relaxation time T_1 was determined by the saturation recovery method using an 80 ns saturating pulse and Hahn-echo detected magnetization amplitude. The magnetization recovery from saturation was single exponential.

The decay of ESE in phase relaxation measurements was weakly modulated, and the T_M time was found to be independent of the pulse length indicating negligible effects of spectral and instantaneous diffusion due to the low Cu^{2+} concentration.

3. Results and discussion

3.1. Cw-EPR spectra and vibronic g-factor averaging

The EPR spectrum of Cu^{2+} in the SrF_2 single crystal observed at low temperatures in a general crystal orientation consists of many narrow lines corresponding to the three magnetically

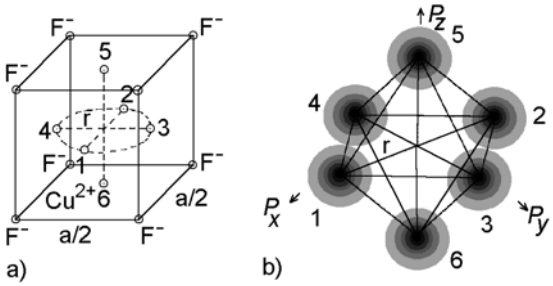

Figure 2. (a) Fluorine cube in the unit cell of an SrF_2 crystal (1/8 of the unit cell with $a = 0.586$ nm) with six off-centre positions of a Cu^{2+} ion replacing the Sr^{2+} ion. (b) The six minima (wells) in the adiabatic potential surface in P_i space ($i = x, y, z$ parallel to the cube edges, see section 3.2).

inequivalent Cu^{2+} sites as expected for six off-centre positions. The lines are further split into hyperfine quartets and ligand superhyperfine lines from four equivalent ^{19}F ($I = 1/2$) nuclei. Because the lines are relatively narrow (about 0.5 mT) the isotope ^{63}Cu, ^{65}Cu splitting is also resolved. The spectrum recorded at 11 K along the [001]-axis, where pulsed EPR experiments were performed, is shown in figure 1(a), and the corresponding field swept electron spin echo (FS ESE) spectrum of the perpendicular region is shown in figure 1(b). The FS ESE spectrum, which is an absorption type EPR spectrum, shows no trace of the broad background component visible in the cw-EPR spectrum. This means that this line is not detectable by ESE because of its very short relaxation time indicating that this is a single homogeneously broadened EPR lines produced most probably by copper(II) clusters.

Angular variations of the spectrum show axial crystal field symmetry at the Cu(II) site, and the spin-Hamiltonian parameters below 30 K (where the parameters are temperature independent, i.e. in the rigid lattice limit) are $g_\parallel = 2.493(2)$, $g_\perp = 2.083(2)$, $A_\parallel(^{63}Cu) = 121 \times 10^{-4}\,cm^{-1}$, $A_\parallel(^{19}F) = 135 \times 10^{-4}\,cm^{-1}$, $A_\perp(^{19}F) = 33.0 \times 10^{-4}\,cm^{-1}$ and quadrupole coupling parameter $Q(^{63}Cu) = 2.7 \times 10^{-4}\,cm^{-1}$. The ground state of Cu^{2+} is d_{xy} (with x, y, z along the crystallographic axes) and the interaction with four equivalent fluorine ions shows that Cu^{2+} ions are located in off-centre positions with an effective C_{4v} crystal field symmetry as shown in figure 2.

The EPR spectra are strongly temperature dependent. The g-factors are constant at temperatures up to 60 K then start slowly but clearly to average (figure 3). This process becomes very rapid above 175 K and leads to a full averaging into a single broad and asymmetric line above 225 K with $g = 2.224(10)$ equal to $\langle g \rangle = (g_\parallel + g_\perp)/3$ within experimental error. The line asymmetry is due to the unresolved isotropic hyperfine structure with a pattern characteristic for the liquid-like dynamics. The averaging of the line positions goes simultaneously with a continuous line broadening (figure 3(b, bottom)) which appears in the whole temperature range in contradiction to the g-factors which are temperature independent below 60 K. Such temperature behaviour is characteristic for vibronic dynamics which mixes ground states of various Jahn–Teller distorted configurations resulting from the off-centre Cu^{2+} positions. The two-step averaging process clearly seen in the g-factor temperature behaviour shows that more than one mechanism of interwell barrier crossing operates. A tunnelling in the ground states may be responsible for the slow g-factor shifts at low temperatures.The fast averaging with final collapse of the spectrum at 225 K must be done by more effective mechanisms which can be either the phonon tunnelling controlled process via an excited vibronic level or overbarrier jumps. Both mechanisms seem to operate in the crystal as will be seen from electron spin–lattice relaxation data discussed in section 3.3.

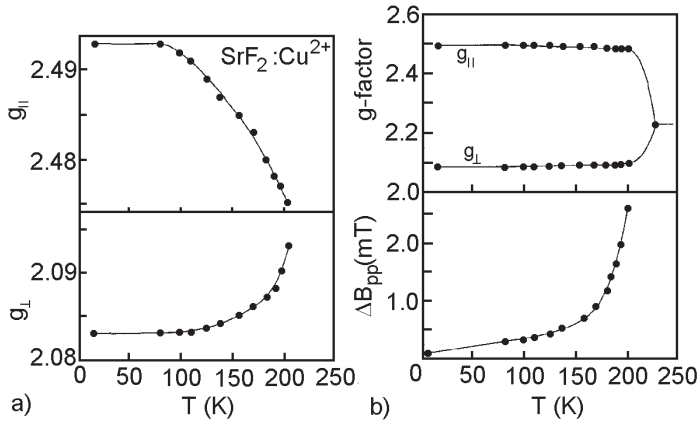

Figure 3. (a) The slow temperature averaging of the g-factors below 200 K. (b, top) The g-factor averaging leading to the single line above 225 K. (b, bottom) EPR line broadening on heating.

3.2. Theoretical description of the off-centre Jahn–Teller effect

The three magnetically inequivalent Cu^{2+} sites with tetragonal crystal field symmetry C_{4v} and the hyperfine interaction with four equivalent fluorine ions clearly show that there are six off-centre positions of the Cu^{2+} ion resulting from a shift of the ion from the centre of the fluorine cube with initial O_h symmetry. The problem of non-central positions of the impurity ions has been considered in many papers. In some of them it was assumed that the non-centrality of an impurity ion with the singlet A_g ground state is due to the pseudo-Jahn–Teller effect. The first to propose the combined Jahn–Teller and pseudo-Jahn–Teller effect for an explanation of the non-centrality were Opik and Pryce [25]. They proposed the $(A_{1g} + T_{2g}) \otimes (a_{1g} + e_g + t_{2g} + t_{1u})$ vibronic coupling scheme but without detailed solution of the problem. This scheme has been more fundamentally studied in a linear approximation by Bersuker and Polinger [26] and by Maaskant and Bersuker [27] although an alternative $(E_g + E_u) \otimes (e_g + e_u)$ scheme has been also proposed [28]. Effects of the third and fourth order anharmonicity were taken into account in description of the experimental results of the SrO:Ni^+ system [29].

Using the above ideas and our experimental data we can propose a scheme of the vibronic interaction for Cu^{2+} in SrF_2 i.e. for Cu^{2+} in eightfold coordination with T_{2g} ground state. Such case has been not considered so far. To define the Jahn–Teller active vibrational modes one should consider at first the direct product $T_{2g} \otimes T_{2g} = A_{2g} + E_g + T_{1g} + T_{2g}$ [30]. The T_{1g} corresponds to a rotation of the copper(II) complex as a whole and may be omitted. The T_{2g} term can be excluded because the trigonal distortion of the complex is not observed in our crystal. Thus only a_{1g} and e_g vibrational modes should be considered as active modes. These modes, however, are able to produce a tetragonal distortion of the complex with on-centre position of the Cu^{2+} ion. To account for an off-central displacement one has to consider a mixing of the ground state of Cu^{2+} with excited configurations. As the ground state of the Cu^{2+} is 2D the vibronic coupling to the odd terms of the excited configurations should be considered. In $3d^84s$ and $3d^84d$ configurations the all terms are even. The odd term is related to the A_{2u} state arising from the ^2F term in excited $3d^84f^1$ configuration.

A tetragonal non-central distortion of the copper(II) complex in O_h symmentry can be created by odd vibrational modes. Thus among the possible a_{1g}, e_g and t_{1u} modes only the

t_{1u} vibrational mode being a linear combination of the t'_{1u} and t''_{1u} modes should be taken into account. The t_{2u} modes are excluded by the symmetry. Thus we can replace the manifold of the excited states by the A_{2u} state coupled to the ground T_{2g} state by the t_{1u} vibrational mode.

The above assumptions are justifies by the following experimental facts: (i) the positive hole in the $3d^9$ ground electronic configuration is localized mainly on the d_{xy} orbital of the impurity ion; (ii) the paramagnetic complex has tetragonal symmetry (C_{4v}) with tetragonal axes along crystallographical fourfold axes; (iii) the motional averaging of the EPR spectrum occurs at relatively high temperatures suggesting deep potential wells. Thus we propose the $(T_{2g}+A_{2u})\otimes(a_{1g}+e_g+t_{1u})$ scheme of the vibronic interaction in the non-central copper complex in the SrF_2 crystal. This scheme means the combined Jahn–Teller and pseudo-Jahn–Teller effect.

In our case the matrix W of the vibronic coupling of the vibrational Hamiltonian $H = T + V + W$ (where T is the kinetic energy of the vibrational modes and is ignored in our calculation, and V is its potential energy) will be represented in the space of four electronic functions. We assume that the ground state T_{2g} with the wavefunctions $|xy\rangle$, $|xz\rangle$ and $|yz\rangle$ is located at the $-\Delta$ position on the energy scale. The excited term $2A_{2u}$ effectively coupled with the ground state triplet T_{2g} is located at 3Δ and has the wavefunction $|xyz\rangle$. Following the paper [27] we can write the potential energy operator in the form containing the harmonic part only

$$V = \tfrac{1}{2}k_0S^2 + \tfrac{1}{2}k_1P^2 + \tfrac{1}{2}k_2U^2 \tag{1}$$

where $P^2 = P_x^2 + P_y^2 + P_z^2$ with components being normal t_{1u} coordinates. Similarly, $U^2 = Q_\Theta^2 + Q_\varepsilon^2$ with e_g coordinates, and S is the breathing normal coordinate of symmetry a_{1g}, and in the spherical angle coordinates

$$P_x = P\cos\chi\sin\gamma \qquad P_y = P\sin\chi\sin\gamma \qquad P_z = P\cos\gamma \qquad Q_\Theta = U\cos\varphi$$
$$Q_\varepsilon = U\sin\varphi.$$

Denoting the vibronic coupling constants as

$$p = \left\langle xyz \left| \frac{\partial H_e}{\partial P_z} \right| xy \right\rangle \qquad e = \frac{1}{2}\left\langle xy \left| \frac{\partial H_e}{\partial P_\Theta} \right| xy \right\rangle \qquad b = \left\langle xyz \left| \frac{\partial H_e}{\partial P_s} \right| xyz \right\rangle \tag{2}$$

we can represent the operators W and V in the reference frame with the origin at the bottom of a potential well and with the electronic Hamiltonian H_e at the equilibrium configuration. For further consideration it is convenient to use the energy units of Δ:

$$S' = \frac{bS}{\Delta} \qquad P'_i = \frac{pP_i}{\Delta} \quad (i = x, y, z) \qquad P' = \frac{pP}{\Delta} \qquad Q'_\alpha = \frac{eQ}{\Delta} \quad (\alpha = \Theta, \varepsilon)$$
$$U' = \frac{eU}{\Delta} \qquad h = \frac{b^2}{k_0\Delta} \qquad f = \frac{p^2}{k_1\Delta} \qquad g = \frac{e^2}{k_2\Delta}$$

where the constants h, f and g are positive.

In this notation

$$V = \frac{(S')^2}{2h} + \frac{(P')^2}{2f} + \frac{(U')^2}{2g} \tag{3}$$

and the W matrix in the $\{|xyz\rangle, |xy\rangle, |xz\rangle, |yz\rangle\}$ basis becomes

$$W = \begin{pmatrix} 3(1+S') & P'_x & P'_y & P'_z \\ P'_x & -1+Q'_\Theta-\sqrt{3}Q'_\varepsilon - S' & 0 & 0 \\ P'_y & 0 & -1+Q'_\Theta-\sqrt{3}Q'_\varepsilon-S' & 0 \\ P'_z & 0 & 0 & -1-2Q'_\Theta-S' \end{pmatrix}. \tag{4}$$

Table 1. Angular positions of the wells in the six-well adiabatic potential surface.

Number of the well	φ (°)	χ (°)	γ (°)
1	0	0	0
2	120	0	90
3	240	90	90
4	120	180	90
5	240	270	90
6	0	0	180

This is a tetragonal pseudo-Jahn–Teller case with six possible minima in a potential surface (six potential wells) defined in table 1 in terms of the angles φ, χ and γ. There are two radial spherical components of U and P being the same for all wells. Four energy levels corresponding to any well can be determined from the equation $\varepsilon = \varepsilon_i' + V$, where ε_i' are the eigenvalues of W:

$$\varepsilon_1' = \varepsilon_2' = (-1 + Q' - S')$$
$$\varepsilon_3' = \varepsilon_4' = (1 + S' - U') \pm \sqrt{\tfrac{1}{4}(4 + 4S' + 2U')^2 + (P')^2}. \tag{5}$$

Thus, the lower sheet of the adiabatic potential surface of the wells is determined by ε_4.

The surface in P_i ($i = x, y, z$) space is shown schematically in figure 2(b) with the depth of wells represented by different degree of shadow. Each well has four adjacent wells located at distance $\sqrt{2}r$ (r is the Cu(II) displacement from the centre of the cube) and one opposite well at distance $2r$. Thus two types of barrier with different heights are expected, with lower barriers between adjacent wells. In the first-order approximation the electronic wavefunctions of the adjacent wells are orthogonal but those belonging to the opposite wells are non-orthogonal. Thus, at low temperatures when predominantly the ground vibronic states are populated, only the tunnelling through the barriers between opposite wells expected. The probability of the tunnelling transitions between lower vibronic states of the opposite adiabatic wells can be estimated using the one-dimensional Gomez–Bowen–Krumhansl model [31], as proportional to the overlap integral $s = \exp(-m\omega\delta^2/\hbar)$ arising from the nuclear wavefunctions of the two lowest levels of the one-dimensional system, where m is the impurity mass, ω is the frequency of oscillations and δ is the barrier width. For the ground state of the $[CuF_8]^{6-}$ complex $\delta \approx 2r_0$, where r_0 is the distance from the centre of the fluoride cube to the equilibrium Cu^{2+} position. Thus, the nuclear motions in each well are independent one from another, and the lowest vibronic energy levels in each well can be considered as equidistant harmonic oscillator levels. These energy levels can be determined from electron spin relaxation data as will be shown in the next section.

3.3. Electron spin–lattice relaxation

The recovery of the magnetization to equilibrium after saturation of the resonance line was single exponential in the whole temperature range and the spin–lattice relaxation time T_1 determined from the fitting of the recovery function was temperature dependent as shown in figure 4(a). T_1 varies continuously from $T_1 = 0.152$ s at 5 K to 4.1×10^{-7} s at 84 K. This is an unusually large increase in the relaxation rate on heating (six orders of magnitude) whereas typically $1/T_1$ increases by no more than four orders of magnitude in this temperature range for Cu(II) complexes. Thus a very efficient mechanism of the spin excitation energy transfer

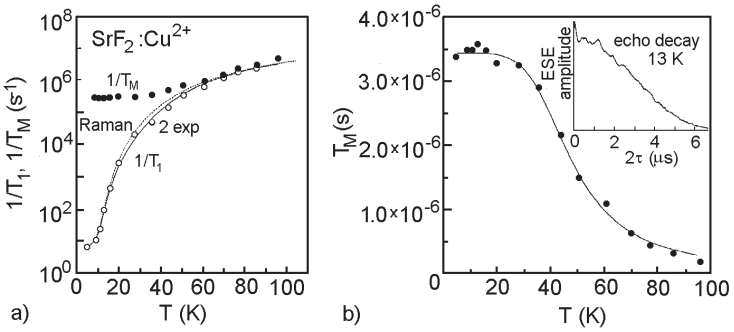

Figure 4. (a) Temperature dependence of the spin–lattice $1/T_1$ and phase $1/T_M$ relaxation rates. The solid line is the best fit of experimental $1/T_1$ data to the two-exponential equation (8) and the dashed line is the best fit to the Raman processes described by equation (6). (b) Temperature dependence of the phase memory time T_M. The solid line is the best fit to the equation (9) assuming that the phase relaxation is governed by spin–lattice relaxation processes.

to the lattice phonons must operate, much more effective than the ordinary phonon scattering Raman processes in other crystals.

The characteristic feature of the Raman processes is that the $T_1(T)$ dependence tends to the limit $1/T_1 \propto T^2$ for $T \geqslant \Theta_D$ (Θ_D is the Debye temperature). Such a limit is not reached in our experiments since we were able to determine T_1 below 90 K only. However, the T_1 experimental data can be fitted to the equation:

$$\frac{1}{T_1} = a + bT + cT^9 \int_0^{\Theta_D/T} \frac{x^8 \exp(x)}{[\exp(x) - 1]^2}\,\mathrm{d}x \tag{6}$$

where the bT term describes the direct one-phonon process, the last term describes the two-phonon Raman process with the transport integral $I_8(\Theta_D/T)$ taken over the Debye-type phonon spectrum and b and c coefficients depend on the details of the relaxation mechanism. The best fit is shown in figure 4(a) by a dashed line with parameters: $a = 0.03\ \mathrm{s}^{-1}$, $b = 1.2\ \mathrm{s}^{-1}\ \mathrm{K}^{-1}$, $c = 8 \times 10^{-9}\ \mathrm{s}^{-1}\ \mathrm{K}^{-9}$ and $\Theta_D = 206\ \mathrm{K} = 180\ \mathrm{cm}^{-1}$. The Debye temperature $\Theta_D = 206$ K, however, is much smaller than Θ_D determined from T_1-relaxation measurements of the atomic H^0 centre in CaF_2 ($\Theta_D = 474$ K) and from calorimetric data [32]. Thus the Raman processes seem to be not responsible for the observed $T_1(T)$ dependence.

In equation (6) it is assumed that the vibronic dynamics is dominated by typical Raman processes as we found lately for Cu^{2+} in Tutton salts with the Jahn–Teller effect [21].

A domination of the ordinary Raman processes over the Jahn–Teller reorientation dynamics in electron spin–lattice relaxation is expected for the case of the static Jahn–Teller effect which can occur at low temperatures for very high interwell barriers or when a system is strongly localized in a deepest potential well by local crystal strains. Generally, however, especially at high temperatures, it is expected that vibronic dynamics can be a very effective mechanism of spin–lattice relaxation. The effectivity of this mechanism depends on the reorientation rate between distorted configurations and on the ability of the reorientations to induce the spin flips.

The coupling between reorientations and the spin flips can be produced: (i) by the direct spin–orbit driven tunnelling [12, 33, 34], or (ii) indirectly by modulations of the hyperfine or g-factor anisotropy [18, 19]. In case (i) the spin–lattice relaxation rate $1/T_1$ is equal to the reorientation rate $1/\tau$, whereas in case (ii) most reorientations are not accompanied by spin flips and the relaxation rate is much slower than $1/\tau$.

The reorientation rate $1/\tau$, i.e. the barrier crossing rate, can be determined by: (1) tunnelling in the ground state with $1/\tau \propto T^7$ in case (i) [34, 36] or $1/\tau = /\Gamma'/^2 T^3$ in case (ii) (Γ' is the tunnelling matrix element in the ground vibronic state) [34–36]; (ii) tunnelling controlled processes via excited vibronic states [33] with $1/\tau = bT^5$ where $b \propto \lambda'$ in case (i) [33] and $b \propto \Delta$ in case (ii) (Δ is the energy of the excited vibronic state) [18, 19, 36]; (iii) phonon induced tunnelling via a virtual phonon state of energy δ_{12} [34, 37] with $1/\tau = c\exp(-\hbar\omega/kT)$ in case (i) ($c = /2\Gamma'/^2\{[1/\delta E + \delta_{12}^2\delta E][1 + \exp(-\hbar\omega/kT)]\}^{-1}$ where δE is the width of the ground energy level and $\hbar\omega$ is vibrational energy) [34], and $1/\tau \propto \delta_{12}T^5$ in case (ii) [18, 19, 36]; (4) overbarrier jumps at high temperatures which are described by the classical rate expression $1/\tau = d\exp(-E_b/kT)$ where E_b is the barrier heights [36].

Moreover the electron spin–lattice relaxation may not be governed by the reorientation rate but may be entirely determined by excitations to an excited vibronic level and recovery back to the ground state in the same potential well. Such a mechanism being the Orbach-type relaxation is possible only due to the mixing of the electronic and nuclear vibrational wavefunctions in the vibronic states of Jahn–Teller systems and does not operate in pure vibrational states. We claim that this mechanism suggested in theoretical work [12] and in our earlier experimental works [20, 21] can be a dominant mechanism of the electron spin–lattice relaxation as well as producing random changes in phase of the spin precessional motion thus accelerating phase spin–spin relaxation. In such a case

$$\frac{1}{T_1} = c\exp\left(-\frac{E_{vibronic}}{kT}\right) \tag{7}$$

where $c \propto \Delta^3$.

The last mechanism i.e. Orbach-type relaxation via an excited vibronic state seems to dominate in our crystal since the experimental data can be well fitted with the expression

$$\frac{1}{T_1} = a + bT + c\exp\left(-\frac{E_1}{kT}\right) + d\exp\left(-\frac{E_2}{kT}\right). \tag{8}$$

The best fit to equation (8) with parameters: $a = 0.03\ s^{-1}$, $b = 1.2\ s^{-1}\ K^{-1}$, $c = 7 \times 10^5\ s^{-1}$, $d = 4 \times 10^7\ s^{-1}$, $E_1 = 120\ K = 83\ cm^{-1}$ and $E_2 = 250\ K = 174\ cm^{-1}$ is shown by a solid line in figure 4(a). The fact that $E_2 = 2E_1$ seems to confirm that relaxation is governed by excitations to the two vibronic levels located within the potential wells of the six off-centre Cu^{2+} positions.

An exponential Orbach-type relaxation in Jahn–Teller systems was reported also for Cu^{2+} in $Zn(BrO_3)_3.6H_2O$ in low temperature measurements (1.2–5 K) with an excited energy state at 3 cm^{-1} [38], and for Cu^{2+} in the $ZnSeO_4.6H_2O$ crystal (4–25 K) with $1/T_1$ described as a sum of three exponential functions with excited level energies 48, 97 and 511 cm^{-1} [39].

3.4. Electron spin–spin phase relaxation

Dephasing of the spin precessional motion after pulse excitation of a inhomogeneously broadened EPR line is described by the phase memory time T_M determined from ESE amplitude decay. The ESE decay of Cu^{2+} in SrF_2 was weakly modulated and well approximated by a single exponential function $V(t) = V_0\exp(-2\tau/T_M)$ where 2τ is the interpulse distance. The phase relaxation rate $1/T_M$ varies with temperature as shown in figure 4(b). This variation is much weaker than $T_1(T)$ and T_1 continuously approaches T_M on heating above 60 K. The experimental $1/T_M(T)$ dependence can be well described as:

$$\frac{1}{T_M} = a_0 + \frac{1}{T_1}. \tag{9}$$

The fit to equation (9) is shown as the solid line in figure 4(b), where the ESE decay at $T = 13$ K is inset. The parameter $1/a_0 = 3.5$ μs is the rigid lattice limit of T_M determined by nuclear spectral diffusion i.e. local magnetic field fluctuations due to dipolar coupling between distant ^{19}F nuclei. An acceleration of the phase relaxation with temperature is entirely done by T_1-processes in the whole measured temperature range. Such a behaviour of T_M can be produced by Jahn–Teller dynamics but not by phonons which can contribute to T_M by Raman processes at much higher temperatures. The strong Jahn–Teller vibronic dynamics is suggested also by a smearing out of the expected fluorine modulations of the ESE decay. Such pronounced modulations were observed for Cr^{2+} in an SrF_2 crystal with the static Jahn–Teller effect at 10 K [24].

An unexpected phase relaxation behaviour, as compared to our data, was reported for the interstitial hydrogen atom H^0 produced in the SrF_2 lattice from OH^- by x-ray irradiation [10, 11]. The rigid lattice T_M value is similar to our data ($T_M = 1$ μs) but the phase memory time is strongly affected by temperature with a characteristic motional-type minimum in the $T_M(T)$ dependence at 60 K. The authors suggest that the minimum is produced by hydrogen atom jumps between off-centre positions along the [110] direction, but more probably it is due to motions of the OH^- impurity located nearby the paramagnetic centre.

3.5. Linewidth and spin relaxation

The continuous although slow increase of phase relaxation rate on heating reflects continuous broadening of the spin packets forming the EPR line. As a result the line broadens and become more homogeneous, and above 84 K the ESE signal vanishes in the dead time of the spectrometer. The spin packet width ΔB_{packed} can be calculated as $\Delta B_{packed} = 1/T_M$ and its temperature variations are compared with the EPR linewidth behaviour in figure 5(a). The spin packet width is temperature independent below 30 K, then continuously increases and for $T > 180$ K the spin packet width becomes comparable with EPR linewidth. This means that in this temperature range the EPR line is homogeneously broadened and the effective relaxation time T_2^* of the whole EPR line can be calculated from the linewidth assuming a Lorentzian lineshape

$$T_2^*[\mathrm{s}] = \frac{13.1302}{g\Delta B_{pp}[\mathrm{mT}]} \times 10^{-9} \tag{10}$$

and

$$\frac{1}{T_2^*} = \frac{1}{T_M} + \frac{1}{2T_1} \tag{11}$$

and simultaneously $T_M \cong T_1$. This allows us to calculate the effective T_1 from ΔB_{pp} for the temperature range where the ESE signal is nondetectable. The results of the calculations are shown in figure 5(b) and compared with previously discussed $T_1(T)$ data. The previously fitted $1/T_1$ dependence presented in figure 4(a) suggests that relaxation should increased more slowly above 100 K whereas the relaxation rate calculated from $\Delta B_{pp}(T)$ indicates that a very effective relaxation mechanism produces a fast increase in the spin relaxation rate. It appears in this temperature range where the rapid averaging of the g-factors begins.

The overall $1/T_1$ experimental data of figure 5(b) can be fitted with equation (8) when an additional term $h\exp(-E_a/kT)$ is added. This term describes jumps over the barriers separating potential wells and h is proportional to the classical oscillation frequency in the well [36]. The best fit to the extended equation (8) is shown in figure 5(b) with $h = 1 \times 10^{13}$ s^{-1} (typical for molecular motions) and $E_a = 2000(90)$ K $= 1750(90)$ cm^{-1} and other parameter values as for the fit in figure 4(a). The energy of the barrier $E_a = 16$ kJ mol^{-1} $= 3.8$ kcal mol^{-1}

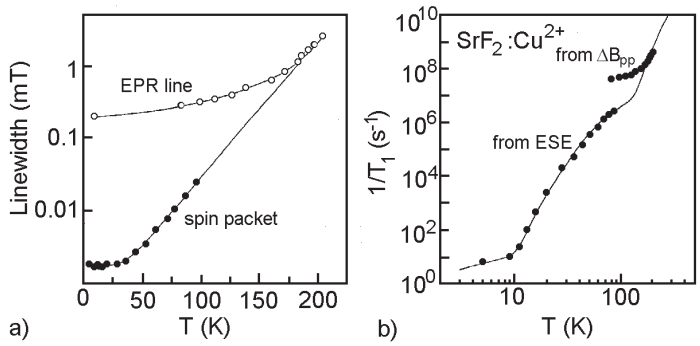

Figure 5. (a) Temperature dependence of EPR linewidth ΔB_{pp} and individual spin packet width (calculated from T_M). Solid lines are the best fits with polynomial expressions. (b) Temperature dependence of the spin–lattice relaxation rate determined by the ESE technique (see figure 4(a)) and calculated from EPR linewidth. The solid line is the best fit with equation (8) with an additional term describing overbarrier jumps (see text).

is rather large compared to the calculated vibronic level energies E_i but it is within typical values of barriers for classical molecular group reorientations in solids.

4. Conclusions

The two-step g-factor averaging, the continuous EPR line broadening on heating and temperature variations of the electron spin relaxation rates allow us to propose a consistent picture of the Jahn–Teller effect and vibronic dynamics of the Cu^{2+} centre in the SrF_2 crystal. The Jahn–Teller effect of the $(T_{2g} + A_{2u}) \otimes (a_{1g} + e_g + t_{1u})$ type produces six off-centre Cu^{2+} positions in the fluoride cube. Below 30 K the static Jahn–Teller effect exists whereas the interwell jumps determine EPR and spin relaxation behaviour at higher temperatures. In temperature range 30–100 K the tunnelling between the potential wells from the ground state and two excited vibronic states of energy 83 cm^{-1}(0.9 kJ mol^{-1}) and 174 cm^{-1}(2 kJ mol^{-1}) governs the spin–lattice and spin phase relaxation and produces the weak g-factor averaging, and continuous EPR line broadening on heating. For higher temperatures the overbarrier jumps produce a full merging of the previously resolved EPR lines into a single broad and homogeneous line and further accelerate the spin relaxation.

Acknowledgment

This work was supported by the Polish Scientific Research Committee under project KBN-2-P03B-122-14.

References

[1] Bill H 1973 *Phys. Lett.* A **44** 101
[2] Bill H 1984 *The Dynamical Jahn–Teller Effect in Localized Systems* ed Yu E Perlin and M Wagner (Amsterdam: North-Holland) ch 13
[3] Zaripov M M and Ulanov V A 1988 *Fiz. Tverd. Tela* **30** 1547
[4] Zaripov M M and Ulanov V A 1989 *Fiz. Tverd. Tela* **31** 254
[5] Alcala R, Alonso P J, Orera V M and den Hartog H W 1985 *Phys. Rev.* B **32** 4158
[6] Oliete P B, Bates C A and Dunn J L 1999 *J. Phys.: Condens. Matter* **11** 2579

[7] Zaripov M M, Tarasov V F, Ulanov V A, Shakurov G S and Popov M L 1995 *Fiz. Tverd. Tela* **37** 806
[8] Zaripov M M, Tarasov V F, Ulanov V A and Shakurov G S 1996 *Fiz. Tverd. Tela* **38** 452
[9] Herrington J R, EstleT L and Boatner L A 1972 *Phys. Rev.* B **5** 2500
[10] Arauzo A B, Orera V M and Alonso P J 1996 *J. Phys. Chem. Solids* **57** 1861
[11] Alonso P J and Arauzo A B 1998 *J. Phys. Chem. Solids* **59** 923
[12] Bill H and Silsbee R H 1974 *Phys. Rev.* B **10** 2697
[13] Pena J I, Alonso P J and Alcala R 1988 *J. Phys. Chem. Solids* **49** 273
[14] Gelhoff W and Ulrici W 1980 *Phys. Status Solidi* b **102** 11
[15] Bersuker I B 1996 *Electronic Structure and Properties of Transition Metal Compounds* (New York: Wiley) ch 9.2
[16] Glinchuk M D 1984 *The Dynamical Jahn–Teller Effect in Localized Systems* ed Yu E Perlin and M Wagner (Amsterdam: North-Holland) ch 14
[17] Bersuker I B 1995 *Ferroelectrics* **164** 75
[18] Williams F I B and Krupka D C 1969 *Phys. Rev.* **179** 255
[19] Ham F S 1972 *Electron Paramagnetic Resonance* ed S Geschwind (New York:Plenum) ch 1
[20] Hoffmann S K, Goslar J, Hilczer W, Augustyniak M A and Marciniak M 1998 *J. Phys. Chem.* A **102** 1697
[21] Hoffmann S K, Augustyniak M A, Goslar J and Hilczer W 1998 *Mol. Phys.* **95** 1265
[22] Rumin N, Vincent C and Walsh D 1973 *Phys. Rev.* B **7** 1811
[23] Goslar J, Hilczer W and Hoffmann S K 1998 *Inorg. Chem.* **37** 5936
[24] Oliete P B, Orera V M and Alonso P J 1997 *Z. Phys. Chem.* **201** 75
[25] Opik U and Pryce F R S 1957 *Proc. R. Soc.* A **238** 425
[26] Bersuker I B and Polinger V Z 1984 *Phys. Status Solidi* b **125** 401
[27] Maaskant W J A and Bersuker I B 1990 *J. Phys. C: Solid State Phys.* **3** 37
[28] Haije W G and Maaskant W J A 1987 *J. Phys. C: Solid State Phys.* **20** 2086
[29] Vikhnin V S and Sochava L S 1979 *Fiz. Tverd. Tela* **21** 2083
[30] Abragam A and B Bleaney 1970 *Electron Paramagnetic Resonance of Transition Ions* (Oxford: Clarendon)
[31] Gomez M, Bowen S P and Krumhansl J A 1967 *Phys. Rev.* **21** 2083
[32] Castle J G and Feldman D W 1997 *Foundations of Modern EPR* ed G R Eaton, S S Eaton and K M Salikhov (Singapore: World Scientific) p 626
[33] Zaritskii I M, Bratus V Ya, Vikhnin V S, Vishnevskii A S, Konthsyts A A and Usintsev V M 1976 *Fiz. Tverd. Tela* **18** 3226
[34] Vikhnin V S 1978 *Fiz. Tverd. Tela* **20** 1340
[35] Pirc R, Žeks B and Gosar P 1966 *J. Phys. Chem. Solids* **27** 1219
[36] Sussmann J A 1967 *J. Phys. Chem. Solids* **28** 1643
[37] Vikhnin V S and Sochava L S 1978 *Fiz. Tverd. Tela* **20** 2412
[38] Jesion A, Shing Y H and Walsh D 1977 *Phys. Rev.* B **16** 3012
[39] Al-Sufi A R, Bulka G R, Vinokurov V M, Kurkin I N, Nizamutdinov N M and Salikhov I X 1993 *Izv. Vyzshykh Utshebnykh Zavied.* 55